Nuclear magnetic resonance imaging of the orbit

IVAN MOSELEY, MICHAEL BRANT-ZAWADSKI, AND CATHERINE MILLS

From the Department of Radiology, University of California, San Francisco, CA 94143, USA

SUMMARY Nuclear magnetic resonance is a noninvasive imaging technique which does not employ ionising radiations. The authors report its application to imaging and tissue characterisation in the normal orbit.

The application of x-ray computed tomography (CT) to the investigation of orbital disease has radically changed the diagnostic approach to patients thought to have retrobulbar masses.[1] Previously available investigative techniques were either relatively uninformative (plain films, phlebography) or potentially hazardous (orbitography).[2] Applications of ultrasound have also developed, but the technique has shortcomings, particularly in disease at the apex of the orbit and in its walls.[3]

X-ray CT also has shortcomings in the orbit: it is relatively nonspecific as regards histology, which is usually inferred from other data.[1] It is expensive to install, and sophisticated studies with modern scanners involve substantial radiation to the eye, which cannot be avoided by screening. The radiation dose, while lower than that of comparable techniques, is still considerable,[4] and recent studies indicate that, with repeated examinations a cataractogenic dose is easily reached.[5]

Nuclear magnetic resonance (NMR) imaging uses no ionising radiation and is very sensitive to tissue differences. At present relatively few centres have the requisite apparatus, but it seems probable that within a few years it will become a major part of the imaging armamentarium. This paper reports preliminary experience of orbital imaging with NMR after a brief explanation of the principles of NMR imaging. More complete reviews of NMR are available for the interested reader.[6–8]

Principles of NMR imaging

Nuclei such as that of hydrogen which have an odd number of protons or neutrons tend when placed in a strong magnetic field to become aligned with that

Correspondence to Dr I. Moseley, Lysholm Department of Radiology, National Hospital, Queen Square, London WC1N 3BG.

field. Hydrogen is present throughout biological tissues and forms the basis for current NMR imaging.

When a radio frequency (RF) pulse is applied to a body in a magnetic field, the protons (hydrogen nuclei) are energised and disturbed from their alignment with it to an extent determined by the amplitude and duration of the pulse. When the pulse ceases, the protons return to their prior alignment, emitting the absorbed energy in the form of an RF signal, which is used to generate the NMR image.

The signal is not identical for all tissues but has an initial intensity and a temporal course characterised by 2 exponential time constants: T1, the 'spin-lattice' constant, and T2 the 'spin-spin' constant. The thermal interaction of the protons with their molecular environment is reflected by T1 as the time taken for the disturbed protons to regain their original alignment with the magnetic field. T2 reflects the fact that, under the influence of the RF pulse, the displaced protons resonate coherently, i.e., repetitively alter their energy state in unison. But, once the pulse ceases, they are influenced by local inhomogeneities in the magnetic field, and the resonance decays. For biological tissues the T1 of protons is generally long, i.e., in excess of 500 ms, while T2 is often less than 60 ms (as measured with an imager working at 3·5 kGauss.)

Although the NMR signal is readily detected, it does not give the spatial information required for imaging. This is achieved, following the suggestion of Lauterbur,[9] by giving the magnetic field a gradient or gradients across the body at the time of sampling, which effectively isolate the desired plane's signal frequency while changing the frequency of the signal from adjacent planes.

Fundamental to current NMR imaging is the possibility of modifying the signal by changing the time which elapses between application of the pulse and sampling (echo delay parameter *a*) and the interval between RF pulses (repetition rate parameter *b*).

Fig. 1   *Spin echo images of normal orbit. In this and subsequent figures, A and B indicate echo delay in ms and repetition interval in seconds respectively. a,b: midaxial section; c: sagittal sections: left: midorbit; upper right: lateral; lower right: medial. A: aqueous; B: plane of ciliary body: BC: buccal cavity; BM: bone marrow; C: cornea; E: ethmoid cells; EF: extraconal fat: F: subcutaneous fat of malar region; G: greater wing of sphenoid; I: inferior rectus and/or oblique muscles; IF: intraconal fat; L: lens; LE: lower lid; LP: lamina papyracea; LR: lateral rectus; LW: lateral wall of orbit; M: maxillary antrum; MR: medial rectus; N: optic nerve; OR: roof of orbit; R: lateral palpebral raphe; S: sclera; SF: Sylvian fissure; SO: superior oblique; SOF: superior oblique fissure; SR: superior rectus; SS: sphenoid sinus; T: tendon of lateral rectus; TF: temporal fascia; TL: temporal lobe; TM: temporalis muscle; UE: upper lid; V: vitreous.*
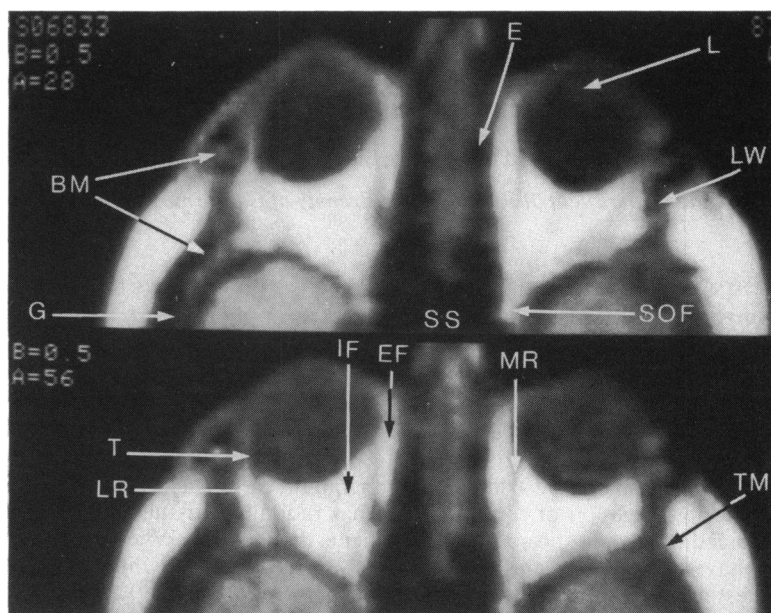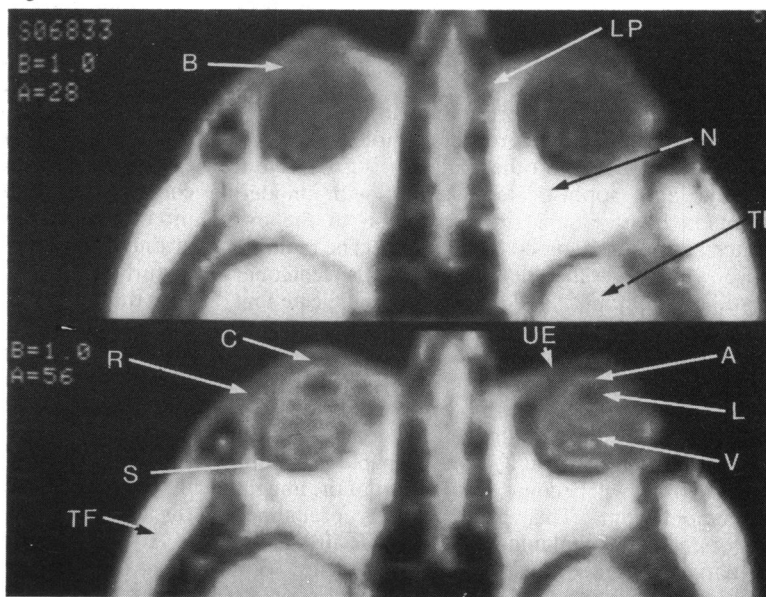
Fig. 1a

Fig. 1b

Variation in these parameters is an essential part of tissue characterisation.[10]

Materials and methods

The NMR studies presented here were carried out at the Radiologic Imaging Laboratory of the University of California, San Francisco, with an imager based on a 3·5 kGauss superconducting magnet, as described by Crooks *et al.*[11] Normal volunteers and patients with no evidence of orbital disease were the subjects. Axial and sagittal images were obtained with a nominal thickness of 7 mm whose central planes were 12 mm apart. A matrix of 128×128 or 256 pixels was used, each pixel having dimensions of approximately 1·5×1·5×7 mm.
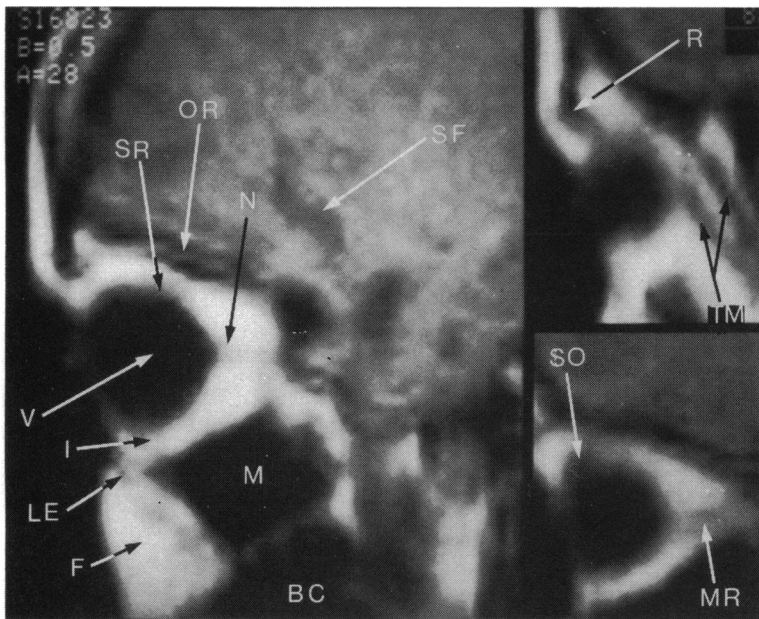
Fig. 1c

Spin echo images were obtained at echo delays (*a*) of 28 or 56 ms, with repetition intervals (*b*) of 0·5, 1·0, or 1·5 s. Since *a* is of the same order as T2, variation in
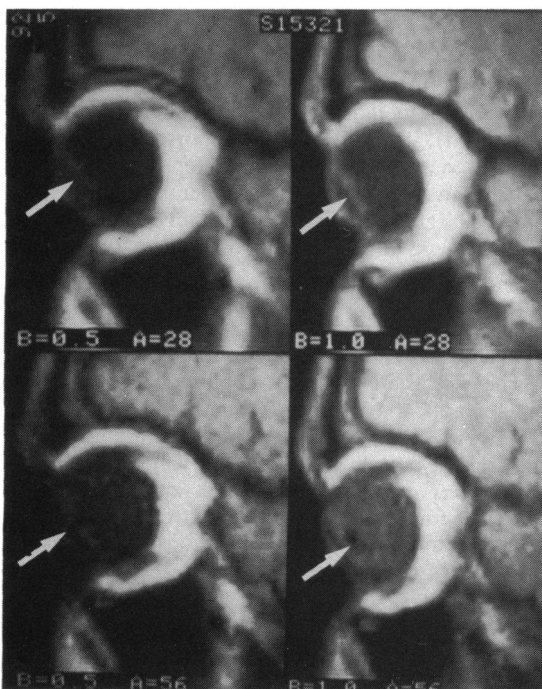

Fig. 2 *Variation in relative signal from media and lens/ciliary body (arrows) with changes in echo delay and repetition rate. Sagittal, midorbital spin echo images.*

echo delay for each plane imaged will reflect the influence of T2 on the tissue's NMR signal, while variations in *b* will produce changes more dependent on T1. Inversion recovery images, with a different RF pulse pattern designed to give images strongly dependent on T1, were also available, with *a*=28 or 56 ms, *b*=1·0 s, and recovery interval=0·4 s.

It has previously been shown that for the spin echo technique used here

$$I = Hf(v) \exp(-a/T2) [-\exp(-b/T1)]$$

where I=intensity of the NMR signal, H=local hydrogen density, *a*, *b*, T1, T2 are as described above, and f(v) is a factor dependent on the velocity of movement of a certain fraction of the hydrogen nuclei through the plane of section.[12] Measurement of I, with variations in *a* or *b*, permits calculation of T2 and T1 respectively.

Relaxation times are apparatus-dependent, varying with strength of the magnetic field and ambient temperature.[13] The present study is therefore concerned on!y with *qualitative* variations in NMR intensity and in calculated T1 and T2 time constants.

Images of NMR intensity are displayed on a grey scale such that the most intense signal from the given section appears white, while very low or absent signals appear black. It is clear from the equation above that tissues with a *long* T2 or a *short* T1 will tend to give intense signals.

Derived images of T1 and T2 can be synthesised by the computer and are similarly displayed in an

Fig. 3 *Inversion recovery images, mid orbit, axial plane. The ciliary body (small arrows) is well seen. Note increased signal from vitreous with longer echo delay (long arrow).*
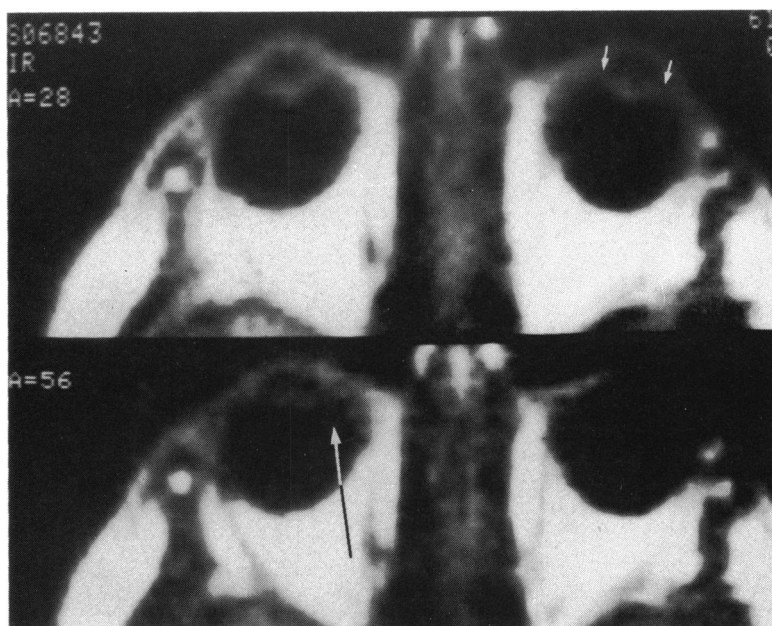
anatomical analogue form, but with the convention that a longer T1 or T2 appears white, while a short relaxation time appears black. Thus, while a *long* T1 is represented in white on a derived T1 image, it will be associated with a lower signal, and therefore a darker area, on a T1 dependent spin echo or inversion recovery image.

Results

NMR IMAGES OF THE NORMAL ORBIT

Normal images are shown in Figs. 1a, b, c. It must be remembered that the factors determining the point on the grey scale of any tissue are quite different from those governing x-ray CT density. Thus, while air is black, as on CT, dense bone, which like most calcified tissues has little hydrogen and gives little or no signal, is also black. In general, densely cellular or fibrous tissues show a weak signal, as do pure liquids with small molecules, which have a long T1.

The major interest of the images lies not in the excellent topographical detail but in the data they contain about the NMR characteristics of normal tissues in vivo.

Images of the eye show the lens, aqueous, vitreous and sclera/cornea.

The *lens* is clearly seen in many images, with a marked change in relative intensity with variations in *a* and *b* (Fig. 2). On spin echo images with *a*=28 ms it is seen as a light grey structure, surrounded by the darker grey of the aqueous and vitreous, but when *a*=56 ms the signal is relatively weak compared with

that of the surrounding media. On inversion recovery images with *a*=28 ms (Fig. 3) the lens shows a strong signal compared to the media, which give virtually no signal, although it is less clearly seen when *a*=56 ms.

Reference to calculated T1 and T2 images (Figs. 4a, b) explains these variations. The lens has a T1 which is only marginally shorter than that of the surrounding media (while much longer than that of orbital fat), but its T2 is much shorter—among the shortest seen in these images. Hence the stronger signal than its environs on T1-dependent images and the weak signal when *a* is progressively longer than its T2. The long T1 is probably a result of the intense cellularity of the lens.

In one adult a small zone of greatly reduced NMR signal was seen within the lens, possibly representing a subclinical calcific focus.

The *ciliary body* is poorly visualised, although some images appear to show a structure having similar NMR properties to the lens but extending further towards the periphery of the globe (Figs. 2, 3).

Aqueous and vitreous have essentially identical NMR characteristics, showing extreme changes in relative intensity with variations in imaging parameters (Fig. 1). On spin echo and inversion recovery images with a short echo delay (*a*=28 ms) signal is almost absent. Increasing *a* to 56 ms increases the signal, as does increasing the repetition interval (*b*) to 1·0 or 1·5 s; when *b*=1·5 s, the intensity of the signal is similar to that of brain (Fig. 5). Images with *b*=2·0 s, not shown here, also show a very strong signal from vitreous.
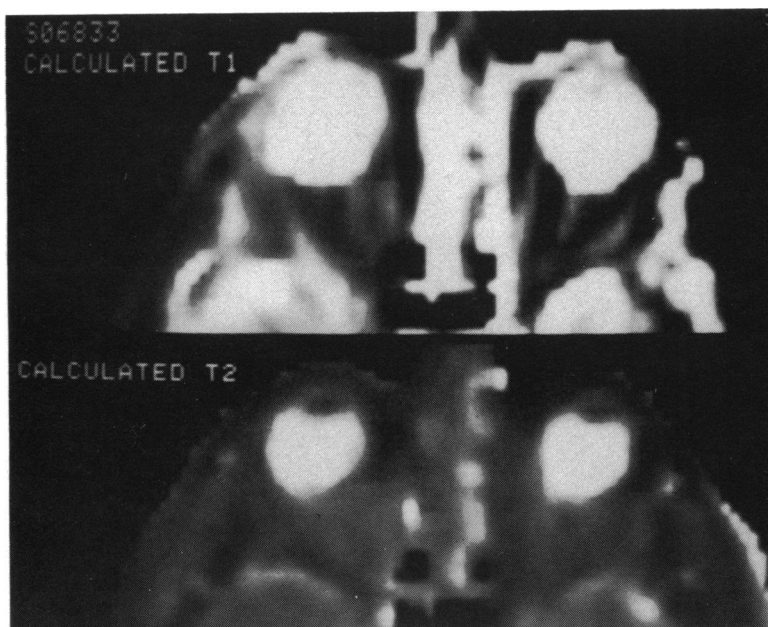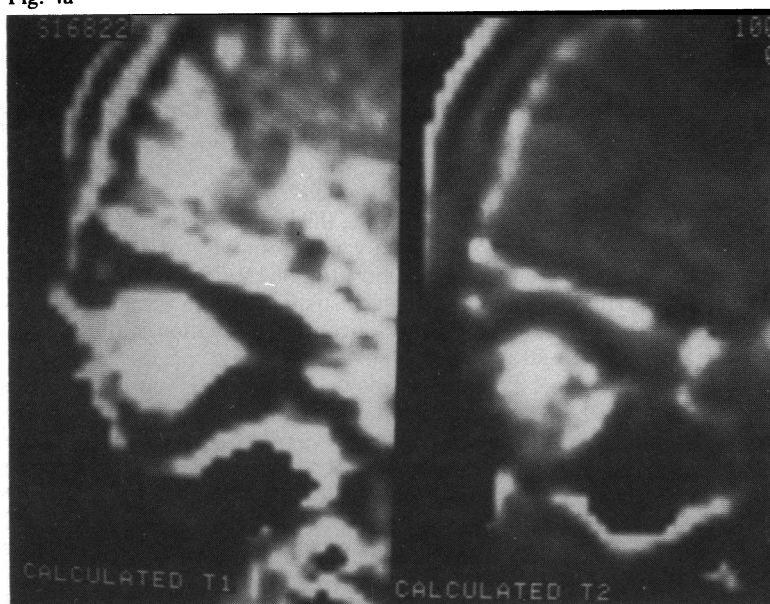
Fig. 4a

Fig. 4 *Images of calculated T1 and T2. a: axial plane (data derived from images in Figs. 1a, b; b: sagittal plane, corresponding to Fig. 1c. In each image a longer relaxation time appears white. Note longer T1 for grey matter than for white in b.*

Fig. 4b

These observations would suggest that both T1 and T2 are long, so that longer *a* and *b* delays would both increase signal. This is borne out by the calculated T1 and T2 images (Fig. 4).

As stated previously, pure aqueous liquids tend to have a long T1. Since vitreous is 98·5% water (plus traces of sodium chloride, protein, and hyaluronic acid) with little or no internal structure, and aqueous

is similar but with even less protein, the finding of a long T1 is not surprising.

Mallard[14] has published in-vivo T1 values, measured from NMR images obtained using a system operating at an RF of 1·7 MHz and with spatial resolution distinctly inferior to that of our apparatus,[15] of 250-300 ms for human brain and spinal cord, 130-160 ms for fat, and 240-260 ms for 'eye.' The

Fig. 5   *Spin echo images with repetition interval of 1·5 s. Note greater contrast between sclera (long arrow) and vitreous and between the tendon of the lateral rectus (arrow) and orbital fat in the lower image.*
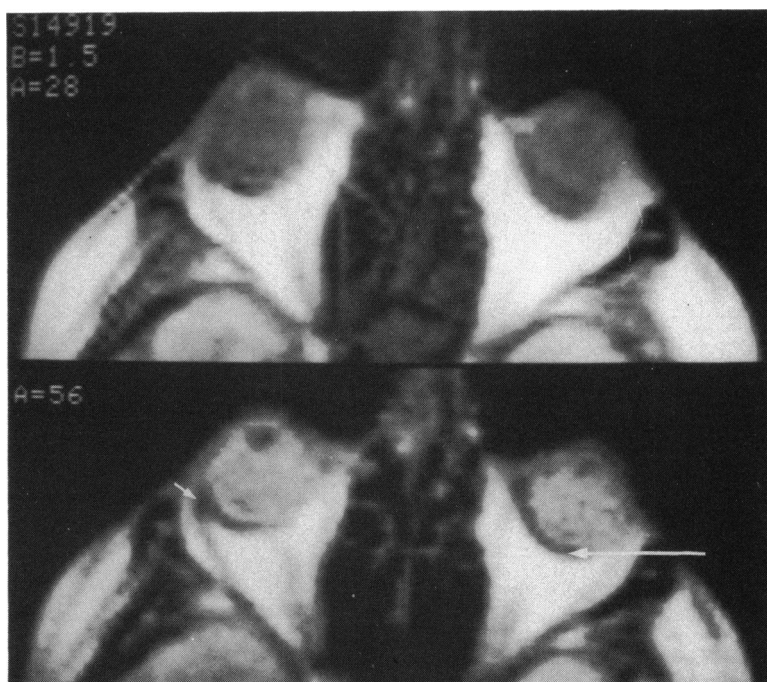
brain and fat values are quantitatively similar to values obtained (in the rat) at the University of California[11]; interspecies differences are small.[16] However, our studies indicate that T1 values for most of the globe are considerably longer than for brain. Images published by Young *et al.*[17] obtained with the free induction decay (FID) technique, which are almost entirely T1-dependent $(I=kH[1-\exp(-b/T1)])$* confirm that the T1 of vitreous is substantially longer than that of brain. The possibility that 'eye' in Mallard's work represented orbital fat is unlikely in view of the very short T1 of fat; moreover, another publication from his group stated that 'paranasal sinuses, orbits, *eyes* and [extra] ocular eye muscles have also been seen.'[15]

The aqueous shows net flow, and 'thermic circulation,' but neither of these are of sufficient magnitude to influence its NMR characteristics.

The *sclera and conjunctiva* also show considerable changes in relative intensity with variation of imaging parameters. They are best seen with long repetition intervals $(b=1·0$ to $2·0$ s) as a fine rim of relatively low signal, most evident posteriorly, where the sclera is known to be thickest. With a short echo delay (28 ms) the sclera is hardly distinguishable from the vitreous, especially anteriorly; there is a suggestion that it gives a slightly stronger signal (Figs 1, 5).

The derived relaxation time images disclose that,

*Transcription of equation given by Young *et al.*[17] into the terms used in this article.

like the vitreous, the sclera has a very long T1, but unlike vitreous it has a short T2. Both of these characteristics confer a weak NMR signal, in keeping with the densely fibrous structure of the sclera and, surprisingly, the cornea.[17]

Anatomically the thickness of retina, choroid, and sclera combined varies from 0·6 to 1·7 mm.[18] Their remarkable demonstration by an NMR imager with a theoretical spatial resolution of only 1·5 mm illustrates the importance of contrast resolution in the demonstration of spatial detail on these images.

Previous workers, including Hounsfield,[19] who reprinted an image first made public in 1978, have published NMR images of the orbit, often with little comment on the eye.[20-22] With the exception of those from this laboratory these have generally been of FID or inversion recovery type, showing the sclera and lens giving a more intense signal than the intraocular media.

The *optic nerve* is shown on both sagittal and axial images (Figs. 1, 5), following a straight or slightly undulating course from the globe to the orbital apex. In all cases the images were obtained in the primary position; it is noteworthy that movement artefacts are lacking, despite the minimum time of 4·3 min for the scanning sequence.

The nerve has a T1 which is considerably longer than that of orbital fat but shorter than that of water. Cerebral grey matter appears to have a substantially longer T1 (Fig. 4), though white matter is in the same
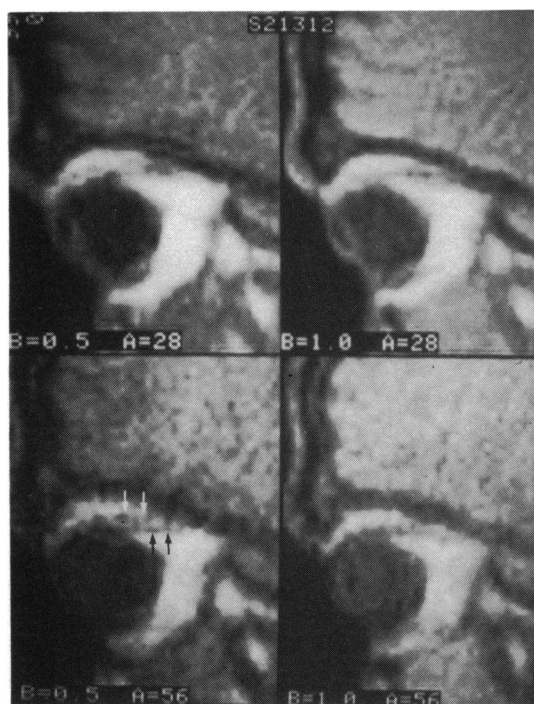
Fig. 6　*Sagittal spin echo images permitting visualisation of superior rectus (black arrows) and levator palpebrae superioris (white arrows).*

Fig. 7　*Sagittal spin echo images showing tendon of superior oblique, which gives little or no signal with all combinations of echo delay and repetition rate.*

range as the optic nerve. It is to be expected that the T1 of the optic nerve would be in the same range as that of the myelinated fibres which make up the white matter but apparently further reduced by inclusion of some orbital fat in the 7 mm thick sections. T2 for the optic nerve is short; visualisation of the nerve was nevertheless improved by increasing both *a* and *b*, both of which decreased the relative signal from the orbital fat.

Axial sections through the upper orbit which include the superior ophthalmic vein and optic nerve in the same 7 mm section show a summation of their shadows, similar to that seen at CT.[23] It is essential that this be recognised and not mistaken for a lesion within the nerve, a possible error which is suggested by the high incidence of optic nerve lesions in some CT studies of suspected multiple sclerosis.[24]

Of the *extraocular muscles*, all 4 rectus muscles are clearly identifiable; sagittal sections also permit distinction of the levator palpebrae superioris (Fig. 6). Images suggestive of the inferior oblique were obtained, and the tendon of the superior oblique muscle is seen fanning out on the superior surface of the globe after passing around the trochlea. Like skeletal muscles the extraocular muscles have a moderately long T1 and a short T2, both of which tend to lead to a faint signal on spin echo and
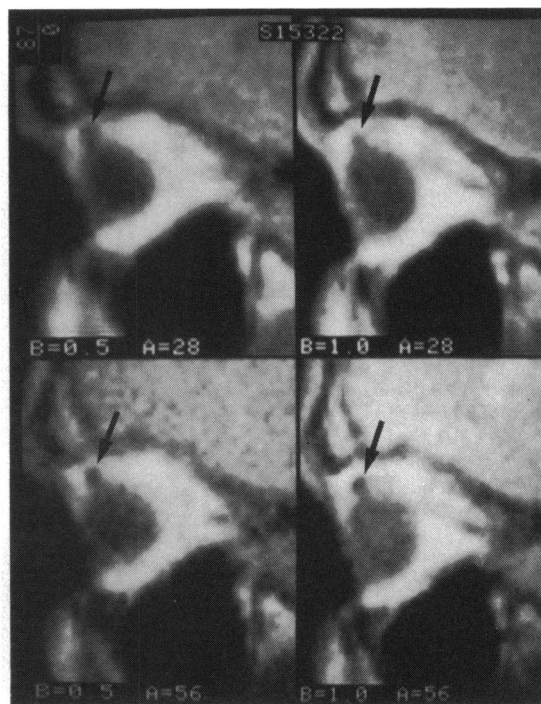
inversion recovery images. Since the orbital fat gives a very strong signal (see below), contrast is high, so that the muscles are well seen despite their size; at 1–2 mm thick, they are at the limits of theoretical resolution. The present studies confirm earlier in-vitro and in-vivo work indicating that the NMR signal from muscle is similar in intensity to that of brain, given the imaging parameters used here.[12–14] As mentioned previously, the eyes have been imaged in the primary position, so that the muscles could be assumed to be in a similar state of contraction. Simple contraction and relaxation of muscle does not appear to affect T1 or T2.[16]

It would be expected that the tendons of the muscles, being more densely fibrous, would give less signal, and there is a suggestion on spin-echo images that this is the case. The tendon of the superior oblique gives a consistently low signal with all combinations of *a* and *b* (Figs. 7, 8). It had previously been suggested on the basis of CT studies that a structure of soft tissue density in this region represented the supratrochlear vein,[25] but the lack of 'enhancement' of the NMR signal (see below) indicates that this is not a vascular structure.

The *orbital fat*, intra- and extraconal, is seen as high intensity with all imaging techniques used in this study. Reference to the calculated T1 and T2 images

Fig. 8 *'Paradoxical enhancement.' In the upper image the superior ophthalmic vein (arrows) appears of the same intensity as the optic nerve, but with a change of parameters it gives a strong signal. The difference is most evident where it crosses the optic nerve (double arrows). The faster-moving blood in the middle cerebral arteries (long arrows) does not show paradoxical enhancement with these parameters. T: tendon of superior oblique; L: lateral check ligament.*
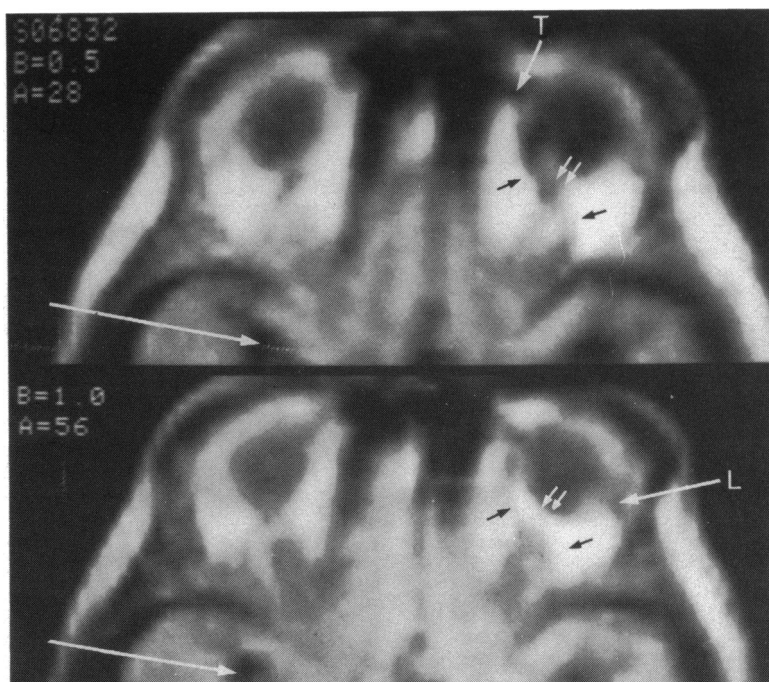
(Fig. 4) shows this is to be the result of a T1 so short that the lack of signal associated with a moderately short T2 is insignificant. Previous in-vitro[13] and in-vivo studies had indicated short relaxation times for fat, e.g. T1=402 ms, T2=50 ms, as compared with 634 and 28 ms for muscle and 643 and 56 ms for brain.[12] Orbital fat is histologically and radiologically indistinguishable from adipose tissue elsewhere.[18]

The *superior ophthalmic vein* is seen clearly in images of the upper orbit (Fig. 8), pursuing its typical serpentine course from the trochlea to the superior orbital fissure. However, it will be noted that when a=28 ms, b=0·5 s, the vein is seen in mid-grey against the white of the fat, whereas when a=56 ms, b=1·0 s, it gives a stronger signal than its surroundings. This variation in the appearance of slowly flowing blood with different NMR parameters was commented on by Young et al.[22] and has been termed 'paradoxical enhancement.'[10] It is a complex phenomenon resulting in part from protons entering and leaving the imaging plane in the interval between application of the RF pulse and sampling.

The *lacrimal gland* is seen as a rather diffuse zone of mottled reduction in intensity of the signal from the orbital fat anterosuperiorly in the lateral part of the orbit, straddling the orbital septum (Fig. 9). The many small secretory lobules of the gland are normally separated by fat, and its borders are rather diffuse.[18] The appearances described here, although, as with x-ray CT,[1] apparently rather disappointing,

nevertheless reflect the structure of the gland.

The *soft tissue planes* around the anterior orbit are very well delineated owing to the high contrast between the fat, fibrous, and muscle planes (Fig. 1).

The *bony walls of the orbit* essentially give no NMR signal; this absence of NMR signal from bone has been described previously.[26] However, the very strong
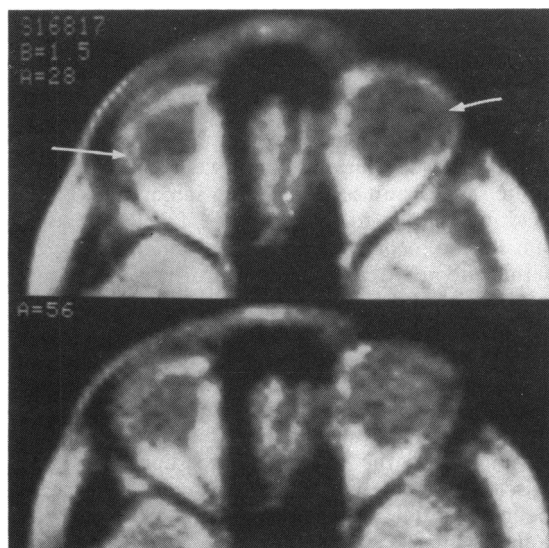

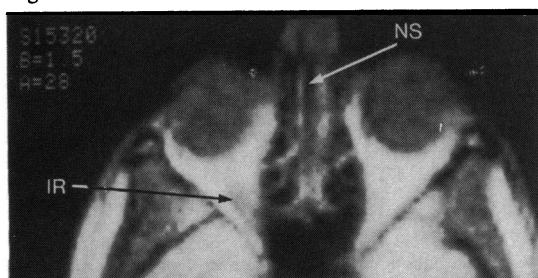Fig. 9 *Spin echo images of upper orbit. Arrows: lacrimal glands.*

Fig. 10a

Fig. 10b

Fig. 10c

Fig. 10 *Spin echo images through* (a) *lower* (b) *mid and* (c) *upper orbit.* GR: *gyrus rectus;* IR: *inferior rectus;* IT: *infratemporal fossa;* NS: *nasal septum.*

signal from fat confers on the marrow spaces a relatively intense signal on both spin echo and inversion recovery images. Marrow is seen to be abundant in the frontomalar region, around the greater wing of the sphenoid, in the supraorbital ridge, and even in the roof of the orbit (Figs. 1, 10a, b, c).

Discussion

It is evident that the spatial and contrast resolution of NMR imaging of the normal orbit is at least as good as that of early, coarse, but clinically valuable, x-ray CT images.[27] Theoretically the magnetic fields and radiofrequency pulses employed should not be injurious, and clinical studies in over 500 children and adults in Aberdeen have not revealed any short-term complications.[28]

The information gained from variations in NMR parameters is fundamental to measurement of tissue

relaxation times and to clinical applications of NMR imaging.[10] Thus the ability to confirm that the superior ophthalmic vein is indeed a vessel, as demonstrated here, requires special programmes and/or the administration of intravenous contrast media when CT is employed. Furthermore, early in-vitro work suggested that relaxation times are different in normal and neoplastic tissues within a single organ.[29]

It must, however, be admitted that poor detail within bone or calcified tissues represents a limitation of the method. Nevertheless, the diagnostic superiority of NMR over CT in some contexts, such as encephalitis, vascular disease, the recognition of areas of demyelination in multiple sclerosis, has already been shown.[30-32] The potential application of NMR imaging to orbital disease is enormous. Laboratory studies have already shown increased relaxation times (particularly T1) in opaque cataractous lenses when the cataract was cortical but not when it was nuclear, reflecting a reduction in the proportion of bound water.[33] The current preliminary studies indicate that intraocular disease should be clearly visible, and the possible detection of changes in relaxation time of tissues which appear radiologically normal, such as the orbital fat in thryoid ophthalmopathy or some cases of orbital granuloma, is exciting. The lack of noxious effects may make it feasible to carry out repeated studies, following the effects of treatment in these and other pathological conditions.

References

1 Moseley IF, Sanders MD. *Computerized tomography in neuro-ophthalmology.* London: Chapman and Hall, 1982.
2 Lloyd GAS. Radiology of the orbit. London: Saunders, 1975.
3 Ossoinig K. Echography of the eye, orbit and periorbital region. In: Arger PH, ed. *Orbital roentgenology.* New York: Wiley, 1977: 224–69.
4 Isherwood I, Pullan BR, Ritchings RT. Radiation dose in neuroradiological procedures. *Neuroradiology* 1977; **16:** 449–53.
5 Lund E, Malaburt M. Irradiation dose to the lens of the eye during CT of the head. *Neuroradiology* 1982; **22:** 181–4.
6 Gadian DG. *Nuclear magnetic resonance and its application to living systems.* Oxford: Clarendon Press, 1981.
7 Kaufman L, Crooks LE, Margulis AR, eds. *Nuclear magnetic resonance imaging in medicine.* Tokyo: Igaku-Shoin, 1981.
8 Pykett JL, Newhouse JM, Buonanno FS, *et al.* Principles of nuclear magnetic imaging. *Radiology* 1982; **143:** 157–68.
9 Lauterbur PC. Image formation by induced local interactions: examples employing nuclear magnetic resonance. *Nature* 1973; **242:** 190–1.
10 Crooks LE, Mills CM, Davis PL, *et al.* Visualization of cerebral and vascular abnormalities by NMR imaging. The effects of imaging parameters on contrast. *Radiology* 1982; **144:** 843–52.
11 Crooks LE, Arawaka M, Hoenninger J, *et al.* Nuclear magnetic resonance whole-body image operating at 3·5 kGauss. *Radiology* 1982; **143:** 169–74.

12 Herfkens R, Davis P, Crooks L, *et al.* Nuclear magnetic imaging of the abnormal live rat and correlations with tissue characteristics. *Radiology* 1981; **141:** 211–8.

13 Ling CR, Foster MA, Hutchison JMS. Comparison of NMR water proton T1 relaxation times of rabbit tissues at 24 MHz and 2·5 MHz. *Phys Med Biol* 1980; **25:** 748–51.

14 Mallard J. The noes have it! Do they? *Br J Radiol* 1981; **54:** 831–49.

15 Edelstein WA, Hutchison JMS, Smith FW, Mallard J, Johnson A, Redpath TW. Human whole-body NMR tomographic imaging: normal sections. *Br J Radiol* 1981; **54:** 149–51.

16 Taylor DG, Bore CF. A review of the magnetic resonance response of biological tissue and its applicability to the diagnosis of cancer by NMR radiology. *J Comput Assist Tomogr* 1981; **5:** 122–34.

17 Young IR, Bailes DR, Burl M, *et al.* Initial clinical evaluation of a whole body nuclear magnetic resonance (NMR) tomograph. *J Comput Assist Tomogr* 1982; **6:** 1–18.

18 Warwick R, ed. *Eugene Wolff's anatomy of the eye and orbit.* 7th ed. Philadelphia: Saunders, 1976.

19 Hounsfield GN. Computed medical imaging. Nobel lecture 8 December 1979. *J Comput Assist Tomogr* 1980; **4:** 665–74.

20 Hawkes RC, Holland GN, Moore WS, Worthington BS. Nuclear magnetic resonance (NMR) tomography of the brain: a preliminary clinical assessment with demonstration of pathology. *J Comput Assist Tomogr* 1980; **4:** 577–86.

21 Doyle FM, Pennock JM, Orr JS, *et al.* Imaging of the brain by nuclear magnetic resonance. *Lancet* 1981; **ii:** 53–7.

22 Young IR, Burl M, Clarke AJ, *et al.* Magnetic resonance properties of hydrogen: imaging the posterior fossa. *AJR* 1981; **137:** 895–907.

23 Moseley IF, Sanders MD, Claveria LE. Diagnostic limitations of computerised tomographic examination of the orbit. In: Bories J, ed. *The diagnostic limitations of computerised axial tomography.* Berlin: Springer, 1978: 52–62.

24 Mastaglia FM, Black JL, Cala LA, Collins DWK. Evoked potentials, saccadic velocities and computerised tomography in diagnosis of multiple sclerosis. *Br Med J* 1977; **i:** 1315–7.

25 Char DM, Norman D. The use of computed tomography and ultrasonography in the evaluation of orbital masses. *Surv Ophthalmol* 1982; **17:** 49–63.

26 Holland GN, Hawkes RC, Moore WS. Nuclear magnetic resonance (NMR) tomography of the brain: coronal and sagittal studies. *J Comput Assist Tomogr* 1980; **4:** 429–33.

27 Gawler J, Sanders MD, Bull JWD, du Boulay GH, Marshall J. Computer assisted tomography in orbital disease. *Br J Ophthalmol* 1974; **58:** 571–87.

28 Smith FW. Safety of NMR imaging. *Lancet* 1982; **i:** 974.

29 Damadian R. Tumor detection by nuclear magnetic resonance. *Science* 1971; **171:** 1151–3.

30 Bydder AM, Steiner RE. NMR imaging of the brain. *Neuroradiology* 1982; **23:** 231–40.

31 Young IR, Hall AS, Pallis CA, *et al.* Nuclear magnetic resonance imaging of the brain in multiple sclerosis. *Lancet* 1981; **ii:** 1063–6.

32 Brant-Zawadzki M, Davis PL, Crooks L, *et al.* NMR in the visualization of cerebral abnormalities: comparison with CT. *Am J Neuroradiol* in press.

33 Pope JM, Chandra S, Balfe JD. Changes in the state of water in senile cataractous lenses as studied by nuclear magnetic resonance. *Exp Eye Res* 1982; **34:** 57–63.